Metabolic models of human gut microbiota: advances and challenges

Daniel Rios Garza[1], Didier Gonze[2], Haris Zafeiropoulos[3,4], Bin Liu[1], Karoline Faust[1 *]

[1] KU Leuven, Department of Microbiology, Immunology and Transplantation, Rega Institute for Medical Research, Laboratory of Molecular Bacteriology, 3000 Leuven, Belgium
[2]Unité de Chronobiologie Théorique, Faculté des Sciences, CP 231, Université Libre de Bruxelles, Bvd du Triomphe, 1050 Bruxelles, Belgium
[3]Biology Department, University of Crete, Heraklion 700 13, Greece
[4]Institute of Marine Biology, Biotechnology and Aquaculture (IMBBC), Hellenic Centre for Marine Research (HCMR), Former U.S. Base of Gournes P.O. Box 2214, 71003, Heraklion, Crete, Greece

[*]Correspondence: karoline.faust@kuleuven.be

Summary

The human gut is a complex ecosystem consisting of hundreds of microbial species interacting with each other and with the human host. Mathematical models of the gut microbiome integrate our knowledge of this system and help to formulate hypotheses to explain observations. The generalized Lotka-Volterra model has been widely used for this purpose, but it does not describe interaction mechanisms and thus does not account for metabolic flexibility. Recently, models that explicitly describe gut microbial metabolite production and consumption have become popular. These models have been used to investigate the factors that shape gut microbial composition and to link specific gut microorganisms to changes in metabolite concentrations found in diseases. Here, we review how such models are built and what we have learned so far from their application to human gut microbiome data. In addition, we discuss current challenges of these models and how these can be addressed in the future.

Why do we need metabolic models of human gut microbiota?

Human gut microorganisms form a complex ecosystem where hundreds of microbial species interact with each other and with the human host. Mathematical models serve to describe this system, to integrate available data and to make predictions of its behavior in different conditions. Given the importance of cross-feeding and competition in the human gut (Louis et al., 2014; Sung et al., 2017), mathematical models applied to the human gut ecosystem need to take into account ecological interactions. The most popular interaction-based model is the generalized Lotka-Volterra model (gLV, (Lotka, 1925; Volterra, 1926)), which describes the change of species abundances over time as a function of their growth rates and pairwise interactions. The gLV model assumes interaction strengths to be constant. However, ecological interactions can be dynamic. For instance, *Escherichia coli* is known to consume acetate when glucose is depleted (Enjalbert et al., 2015). This

switch from one carbon source to another in response to scarcity is known as diauxic shift (Monod, 1949). If another gut bacterium supplies acetate, a cross-feeding interaction can take place at low but not at high glucose levels. In addition, gut bacteria can change their metabolism in response to interaction partners (D'hoe et al., 2018). The gLV model, which does not describe interaction mechanisms, cannot account for this metabolic flexibility.

Whether or not metabolites are considered explicitly in community models has implications for the conclusions derived from analytical or numerical studies of such models. For instance, community stability was stated to depend on the number of species and their interactions (May, 1972) and on the proportion of negative versus positive interactions (Coyte et al., 2015). Butler and O'Dwyer investigated the stability of communities with a consumer-resource model, which describes the community as a set of consumers competing for resources (for instance Bacteroides species competing for carbohydrates). They proved that for this system, any feasible solution (i.e. one with positive abundances for all species) is always stable in the sense of being robust to small perturbations (Butler and O'Dwyer, 2018). This contrasts with the finding that a larger number of species or of interactions in random species interaction matrices increases instability (May, 1972). Butler and O'Dwyer also included producers, which allowed modeling mutualistic interactions through mutual cross-feeding of resources. In this extended consumer-producer-resource model, mutualistic interactions do not necessarily destabilize the system as in gLV-based models (where they can lead to explosive growth) but can give stable solutions in specific cases.

Modeling metabolites explicitly also matters when predicting system behavior. For instance, Momeni and colleagues showed that the gLV model fails to describe the dynamics of two species competing for one metabolite while cross-feeding a second one (Momeni et al., 2017). Finally, metabolic flexibility questions the previously postulated universality of microbial interaction networks (Bashan et al., 2016), since it implies that microorganisms can change their interactions depending on the presence of other species. Due to its simplicity, relatively small number of parameters and ease of handling large species numbers, the gLV is widely used to model the dynamics of microbial communities. However, its inability to handle flexible metabolic responses means that in many cases it does not meet Einstein's famous "as simple as possible but not simpler" criterium. Here, we will present metabolite-explicit modeling approaches[1] as alternatives to gLV model, review the insights resulting from their application to human gut microbiota and discuss their challenges.

How do we include metabolic information?

Metabolic information can be included at different levels of resolution. Depending on the available data and the question, the internal metabolism of a cell can be modeled explicitly or treated as a black box. Kinetic models follow the latter strategy and simplify the system further by focusing on

[1]So far, we used the term 'metabolic model' in a wide sense to refer to all modeling approaches that explicitly account for metabolites. To be more precise, we will use 'metabolite-explicit model' in the remainder of this perspective instead and employ 'metabolic model' only in its narrow sense of genome-scale metabolic model.

growth-limiting nutrients. The generic kinetic equation for a microorganism growing on a single growth-limiting substrate in a chemostat is:

$$\frac{dX}{dt} = \mu(S)X - X$$

$$\frac{dS}{dt} = -\frac{\mu(S)}{Y_{X/S}}X + \Phi(S_{in} - S)$$

where X is the biomass, S the concentration of the nutrient, $Y_{X/S}$ the yield, ϕ the flow rate, and S_{in} the concentration of the nutrient in the inflowing medium. At high nutrient concentrations, the growth rate is no longer limited by nutrient availability but rather by the speed of the processes involved in cell division or the enzyme-limited rates of biochemical reactions and thus the effect of nutrients on the growth rate becomes negligible. This saturation effect is commonly expressed with the Monod function:

$$\mu = \mu_{max}\frac{S}{K + S}$$

where K is the half saturation constant or Monod constant. When several limiting substrates are present, kinetic models require knowledge on the logic of nutrient use, as described in Figure 1. This logic usually needs to be established through experiments (D'hoe et al., 2018; Schmidt et al., 2011).

The consumer-resource model was first introduced to describe resource competition (MacArthur, 1970) and has since been adapted to model production and consumption of metabolites in microbial communities (Marsland et al., 2020). It relies on the additivity assumption and can be seen as a simplified kinetic model. As such, it does not fully capture the metabolic logic that characterizes the behavior of many microorganisms but can be scaled up more easily to large communities.

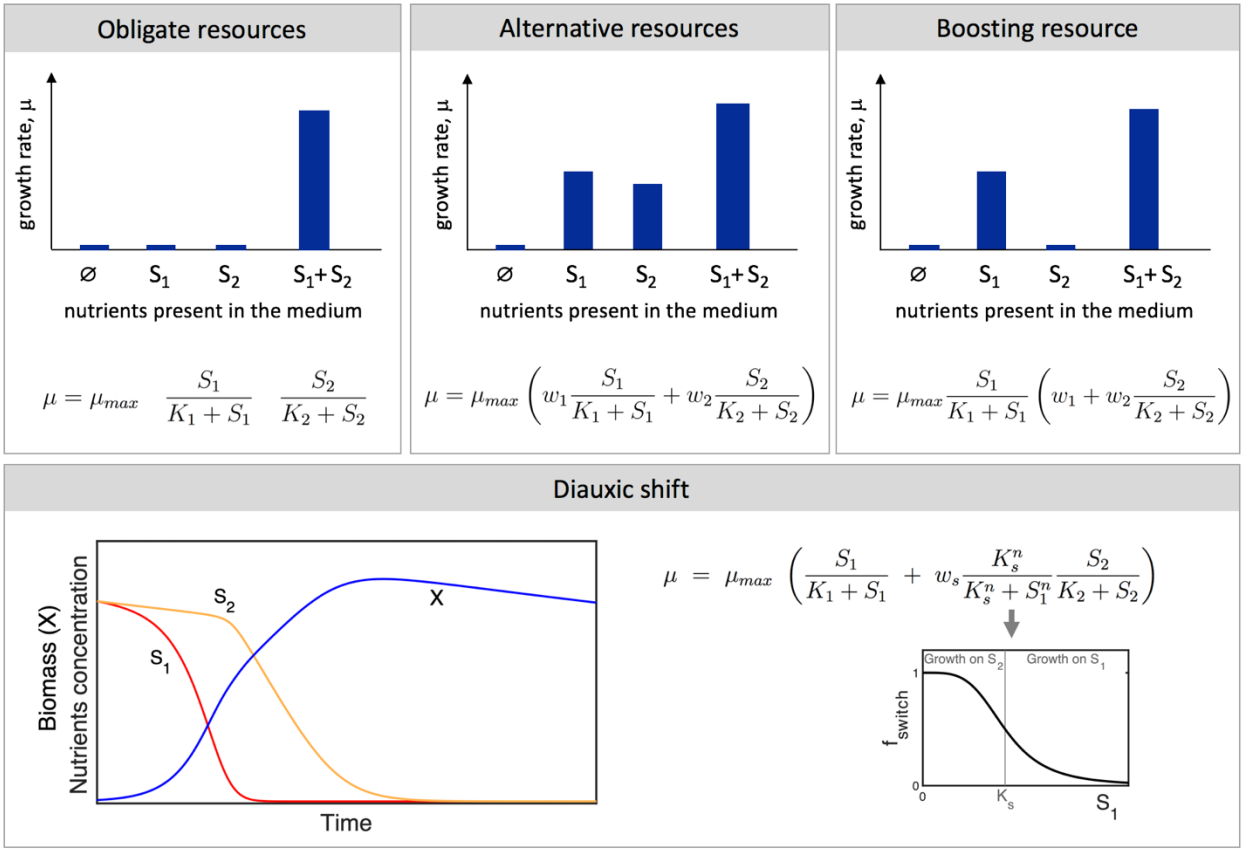

Figure 1: Kinetic models need parameters such as the maximal growth rate μ_{max} and the Monod constant. They also require knowledge on whether a nutrient is required (obligate), whether it can be replaced by another (alternative) and, if this is not the case, whether another nutrient can still boost growth. The lower panel illustrates how kinetic models can implement diauxic shifts. Function f_{switch} expresses the switch from growth on S_1 (when S_1 is high) to growth on S_2 (when S_1 goes below threshold K_s).

While kinetic models require knowledge on metabolic behavior, the promise of genome-scale metabolic models (GEMs) is that such knowledge can be derived ab initio from the genome. During metabolic reconstruction, enzyme-coding genes are identified and linked to reactions, resulting in a stoichiometric matrix A that represents the metabolic network of the cell. While automated metabolic reconstruction can be carried out in minutes (using pipelines such as ModelSEED (Seaver et al., 2021)), high-quality metabolic reconstruction requires manual curation that can take months (Thiele and Palsson, 2010). In a metabolic network, the rate of change in metabolite concentrations is expressed as a linear equation system:

$$\frac{dS}{dt} = Av$$

where S is the vector of metabolite concentrations, A is the stoichiometric matrix and v is a vector of reaction fluxes. Flux balance analysis (FBA) assumes that intracellular metabolites are at steady state, such that their net sum is zero:

$$\frac{dS}{dt} = Av = 0$$

For most metabolic networks, this system contains more unknowns (i.e. fluxes) than equations and has thus an infinite number of solutions. FBA overcomes this challenge by assuming that the cell optimizes fluxes according to certain criteria such as maximizing the production of ATP molecules or the flux through an (artificial) biomass reaction that represents cell growth. These criteria are defined in the objective function (z). Additional constrains are given by limiting reaction fluxes to a range that is biologically feasible. A solution is then found by linear programming.

Since standard FBA assumes a steady state, it cannot model situations where nutrient concentrations change, e.g. in batch processes. Dynamic FBA was introduced to overcome this limitation (Henson and Hanly, 2014; Mahadevan et al., 2002). It describes changes in biomass and substrates with ordinary differential equations (ODEs), which are coupled to static FBA through growth rate (i.e. flux through the biomass reaction) and substrate production and consumption rates. FBA solutions are computed iteratively for each time step to update these rates. Thus, dynamic FBA can be seen as a combination of FBA and a kinetic model.

FBA was designed for single species, but both static and dynamic forms of FBA have been extended to communities (recently reviewed in (Heinken et al., 2021)). As in kinetic models, ecological interactions between species are modeled through nutrient production and consumption, which allows describing commensalism (cross-feeding), mutualism (mutual cross-feeding) and competition. Community FBA approaches can be classified according to their flux optimization strategy into (*i*) group, (*ii*) individual and (*iii*) data-driven approaches (Figure 2A). A straightforward implementation of the first strategy is to select species-specific growth rates such that they maximize a weighted sum across all community members (Stolyar et al., 2007). A generalization of this idea is to compute the Pareto front by fixing the flux through the biomass reaction of one species while optimizing the flux through that of the other species and vice versa for a range of biomass flux values. The point on the Pareto front giving the largest combined biomass flux corresponds to the Pareto-optimal solution (Budinich et al., 2017; Heinken et al., 2013). The idea of optimizing the community biomass is also implemented in CASINO (Shoaie et al., 2015) and SteadyCom (Hung et al., 2017). The second group of community FBA tools optimizes the flux distribution of each species independently of the other species, i.e. without a community-level objective function (Dukovski et al., 2021; Popp and Centler, 2020; Zhuang et al., 2011). Finally, tools such as the Microbiome Modeling Toolbox and MICOM optimize growth rates such that observed species proportions are reproduced (Baldini et al., 2019; Diener et al., 2020).

The assumption that the metabolic network optimizes an objective function can also be relaxed. For this, the space of all conditions that sustain growth can be explored by taking uniform samples from the viable fluxes (Herrmann et al., 2019; Schellenberger and Palsson, 2009), as illustrated in Figure 2B.

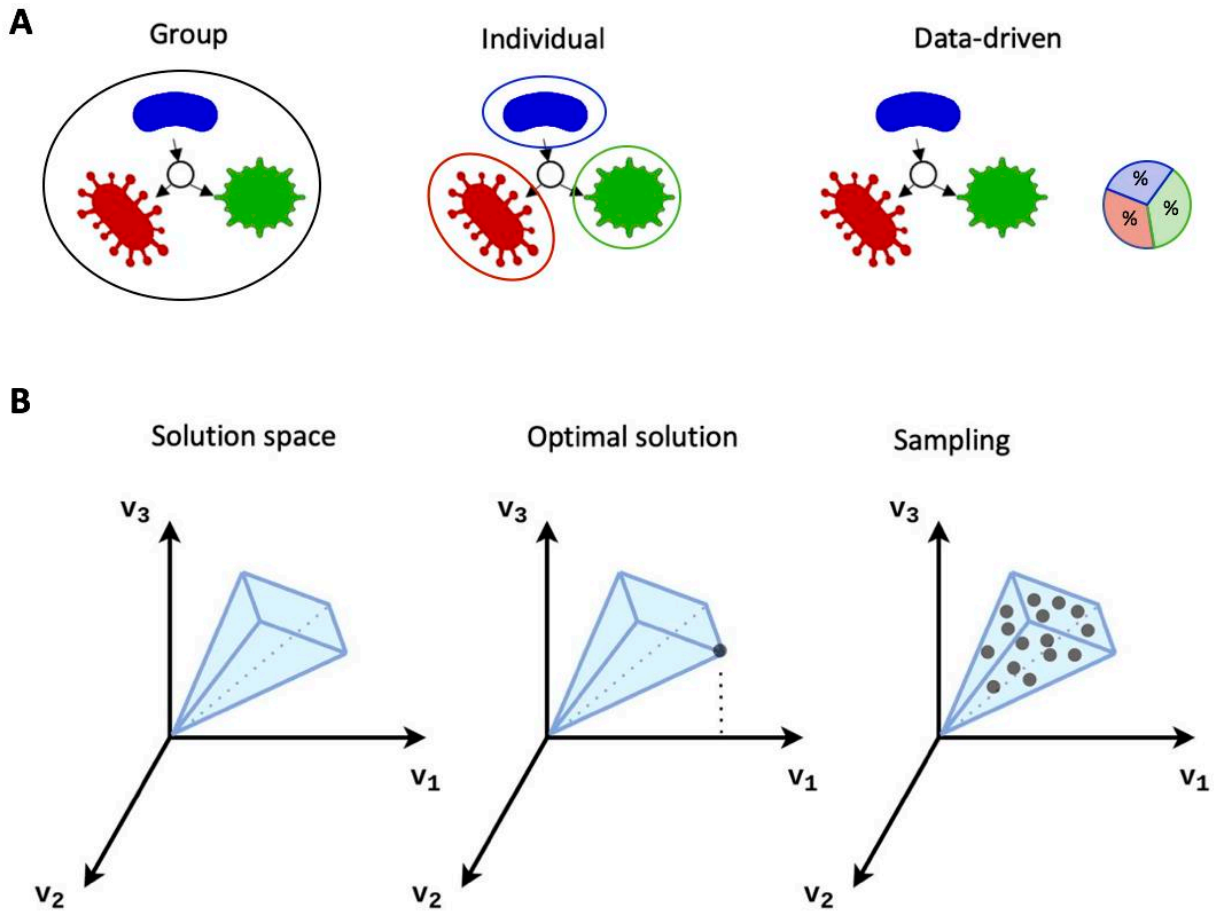

Figure 2: A) Community FBA represents ecological interactions between species indirectly through metabolite production and consumption. There are three strategies to optimize flux distributions in communities: by optimizing both individual and group-level growth rates (group), by only optimizing individual growth rates (individual) and by optimizing growth rates such that measured proportions are reproduced (data-driven). B) FBA finds the point in the solution space of flux distributions that optimizes an objective function, usually growth rate (i.e. the flux through the artificial biomass reaction). In contrast, flux sampling finds random flux distributions in the solution space, which allows estimating the probability distribution for each of the fluxes.

Table 1 summarizes metabolite-explicit modeling techniques that have been applied to human gut microbiota. Three modeling approaches, namely kinetic modeling, dynamic community FBA and flux sampling, are also illustrated in Box 1 on a toy model featuring three artificial gut bacteria, each representing a metabolic niche (carbohydrate degrader, butyrate producer and acetogen).

Box 1: Toy model

To illustrate different metabolite-explicit modeling approaches, we consider simplified representatives of three functional groups found in human gut microbiota, namely a carbohydrate fermenter, an acetogen and a butyrate producer, which are co-cultured in chemostat (A). They all require and thus compete for glucose, which is continuously supplied in the chemostat. The carbohydrate fermenter produces acetate and formate, the former of which is consumed by the

butyrate producer and the latter by the acetogen. In addition, the acetogen and the butyrate producer mutually cross-feed: the acetogen produces acetate that boosts the growth of the butyrate producer, while the latter releases carbon dioxide (and hydrogen), which provides an alternative to formate as obligatory second carbon source for the acetogen.

This system can be described with a kinetic model in the form of ordinary differential equations (ODEs, B). Numerical integration of these ODEs gives the dynamics of each variable (C). The kinetic model can also be used to predict species abundances as a function of control parameters, e.g. the flow rate (D). Parameter values are given in Supplementary Table 1.

A

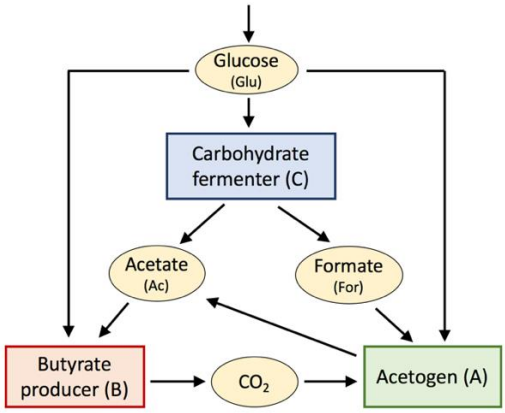

B

$$\begin{aligned}
\frac{dC}{dt} &= \mu_1(Glu)\ C - \phi\ C \\
\frac{dB}{dt} &= \mu_2(Glu, Ac)\ B - \phi\ B \\
\frac{dA}{dt} &= \mu_3(Glu, For, C0_2)\ A - \phi\ A
\end{aligned}$$

$$\begin{aligned}
\mu_1 &= \mu_{max1}\frac{Glu}{K_{11}+Glu} \\
\mu_2 &= \mu_{max2}\frac{Glu}{K_{21}+Glu}\left(1+w_{22}\frac{Ac}{K_{22}+Ac}\right) \\
\mu_3 &= \mu_{max3}\frac{Glu}{K_{31}+Glu}\left(w_{33}\frac{For}{K_{33}+For}+w_{34}\frac{C0_2}{K_{34}+CO_2}\right)
\end{aligned}$$

C

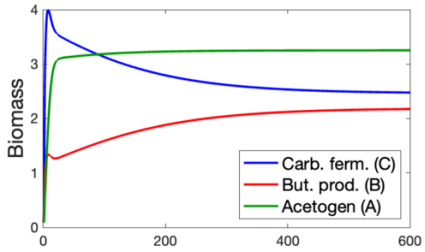

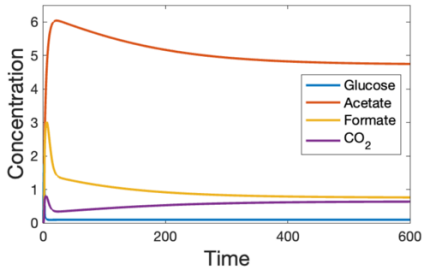

$$\begin{aligned}
\frac{dGlu}{dt} &= \phi\ Glu_{in} - \frac{\mu_1}{Y_{11}}C - \frac{\mu_2}{Y_{21}}B - \frac{\mu_3}{Y_{31}}A - \phi\ Glu \\
\frac{dAc}{dt} &= \alpha_{12}\mu_1 C + \alpha_{32}\mu_3 A - \frac{\mu_{max2}}{Y_{22}}w_{22}\frac{Glu}{K_{21}+Glu}\frac{Ac}{K_{22}+Ac}B - \phi\ Ac \\
\frac{dFor}{dt} &= \alpha_{13}\mu_1 C - \frac{\mu_{max3}}{Y_{33}}w_{33}\frac{Glu}{K_{31}+Glu}\frac{For}{K_{33}+For}A - \phi\ For \\
\frac{dCO_2}{dt} &= \alpha_{24}\mu_2 B - \frac{\mu_{max3}}{Y_{34}}w_{34}\frac{Glu}{K_{31}+Glu}\frac{CO_2}{K_{34}+CO_2}A - \phi\ CO_2
\end{aligned}$$

D

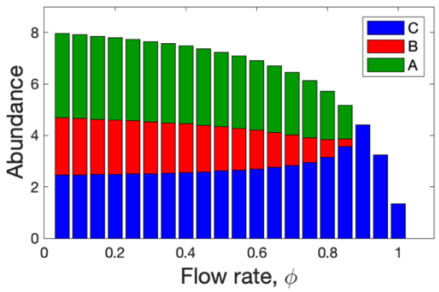

To investigate intracellular fluxes, a metabolic model of the system is needed. For this, we designed simplified metabolic networks for each species (Supplementary Figure 1). The optimal steady-state fluxes (E) were computed with flux balance analysis given ATP production, NAD+ recycling, and coA

acetylation as toy biomass objective functions (Supplementary Table 2), while possible flux distributions are explored with flux sampling (F). Figure G displays the composition for six permutations of the community and the resulting scaled biomass fluxes and metabolic environment predicted with MAMBO (Garza et al., 2018). Dynamic flux balance analysis (H) describes the change of species abundances and metabolite concentrations over time (I), which in this toy system are qualitatively similar to those found with the kinetic model (D). However, the growth rates and metabolite interdependencies emerge from the reconstructed networks.

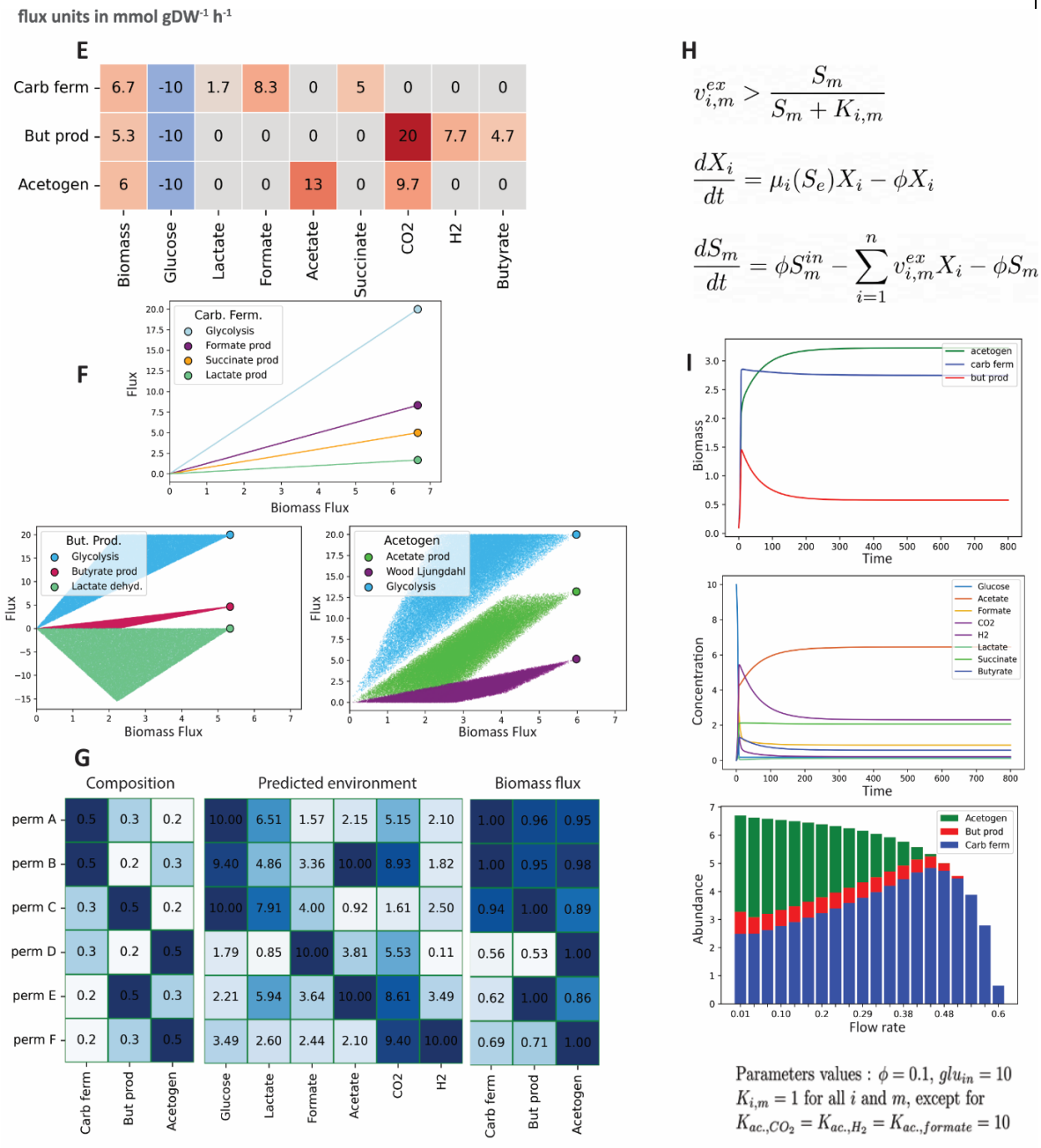

Table 1: Summary of metabolite-explicit community model approaches applied to human gut microbiota. The list of tools given for each modeling approach is not exhaustive.

Model input and output	What can we learn from the model	Tools	Comments	Main limitations
Flux Balance Analysis Input: a stoichiometric matrix per species representing its metabolism; constraints on fluxes; medium definition Output: flux distribution of each species optimizing an objective function, for dynamic FBA: flux distribution of each species (optimal at current time point) and metabolite concentrations over time	- Individual growth rates at steady state and resulting community composition for a given medium - Internal fluxes, production and consumption rates and external metabolite concentrations derived from these - dFBA: community dynamics	- SteadyCom (static FBA, (Hung et al., 2017)) - CASINO (bi-level optimization, (Shoaie et al., 2015)) - Microbiome Modeling Toolbox (Pareto optimality and fit to observed abundances, (Baldini et al., 2019)) - MICOM (optimization to fit observed abundances) - BacArena and COMETS (dynamic FBA on a grid, (Bauer and Thiele, 2018; Dukovski et al., 2021)) - µBialSim and DMMM (optimization of each species independently of the others in a dynamic FBA, (Popp and Centler, 2020; Zhuang et al., 2011))	- Can be embedded in a spatial structure (e.g. (Chan et al., 2019; Hoek and Merks, 2017))	- Depends on correct reaction annotations - Depends on an objective function - Dynamic FBA requires kinetic parameters
Sampling-based approaches Input: a stoichiometric matrix per species representing its metabolism, species	- High probability flux distributions - Degree of certainty of FBA predictions - Metabolome	- optGpSampler (Megchelenbrink et al., 2014) - CHRR (Haraldsdóttir et al., 2017) - MAMBO (samples fluxes to fit observed	- Often applied to single species - May include specific scenarios (e.g. distribution that best explains experimentally measured growth rates (Martino et al.,	- Depend on correct reaction annotations - Computationally challenging - Depend on paired metabolite

abundances or growth rates for MAMBO Output: a set of possible flux distributions from the solution space	that best explains the species distribution	species abundances to predict metabolite concentrations, (Garza et al., 2018))	2018)	and composition data for validation
Consumer-resource model Input: matrix of uptake and production rates for each metabolite per species, growth rates, initial metabolite concentrations and species abundances Output: microbial abundances and concentrations of key metabolites over time	- Prediction of community composition and metabolite concentrations	- Trophic model (coupled consumer-resource models, (Wang et al., 2019)) - Community simulator (Marsland et al., 2020)	- Mostly used qualitatively (e.g. (Butler and O'Dwyer, 2018; Niehaus et al., 2019)) - Special case of the kinetic model	- Depends on biochemical knowledge of each species or functional group - Requires kinetic parameters - Does not take into account metabolic flexibility
Kinetic model Input: knowledge on essential and boosting nutrients and metabolite production, growth rates, initial metabolite concentrations and species abundances Output: microbial abundances and concentrations of key metabolites over time	- Prediction of community composition and metabolite concentrations	- microPop (kinetic model of functional groups in human gut microbiota, (Kettle et al., 2018)) - Spatial extension of microPop (Smith et al., 2021)	- Can be embedded in a spatial structure through compartments or partial differential equations (e.g. (Muñoz-Tamayo et al., 2010))	- Depends on biochemical knowledge of each species or functional group - Requires kinetic parameters - Does not account for internal fluxes
Topological metabolic model Input: metabolic	- Prediction of media supporting	- NetCmpt and NetCooperate (compute	- Applied in combination with co-occurrence to fecal	- No quantitative predictions

network of each species Output: seed set (metabolites not produced by the network) for each organism; can be used to compute interaction potential	growth - Prediction of cross-feeding and competitive relationships from metabolic complementarity or overlap - Identification of key species carrying out bottleneck reactions	competitive and cooperative potential, respectively, (Kreimer et al., 2012; Levy et al., 2015)) - Metage2Metabo (Belcour et al., 2020)	metagenomics data to assess prevalence of habitat filtering (Levy and Borenstein, 2013)	

What did we learn from metabolite-explicit models of human gut microbiota?

Human gut microbial composition varies along the entire human gastrointestinal tract of each individual (Zhang et al., 2014). The small intestine is dominated by bacterial species of the families *Lactobacillaceae* and *Enterobacteriaceae* (Donaldson et al., 2016) while the colon with slower transit time is enriched in more densely growing and diverse species of the families *Bacteroidaceae*, *Prevotellaceae*, *Rikenellaceae*, *Lachnospiraceae* and *Ruminococcaceae*, which are capable of breaking down resistant polysaccharides derived either from the insoluble dietary fiber or colon mucus (Donaldson et al., 2016; Sauvaitre et al., 2021; Zhang et al., 2014). The gastrointestinal system provides microhabitats, such as the lumen of the large intestine, mucus layers and colonic crypts, which feature distinct microbiota (Tropini et al., 2017). Figure 3 summarizes the factors shaping gut microbiota that are considered in the models discussed below. Different models emphasize different subsets of these factors.

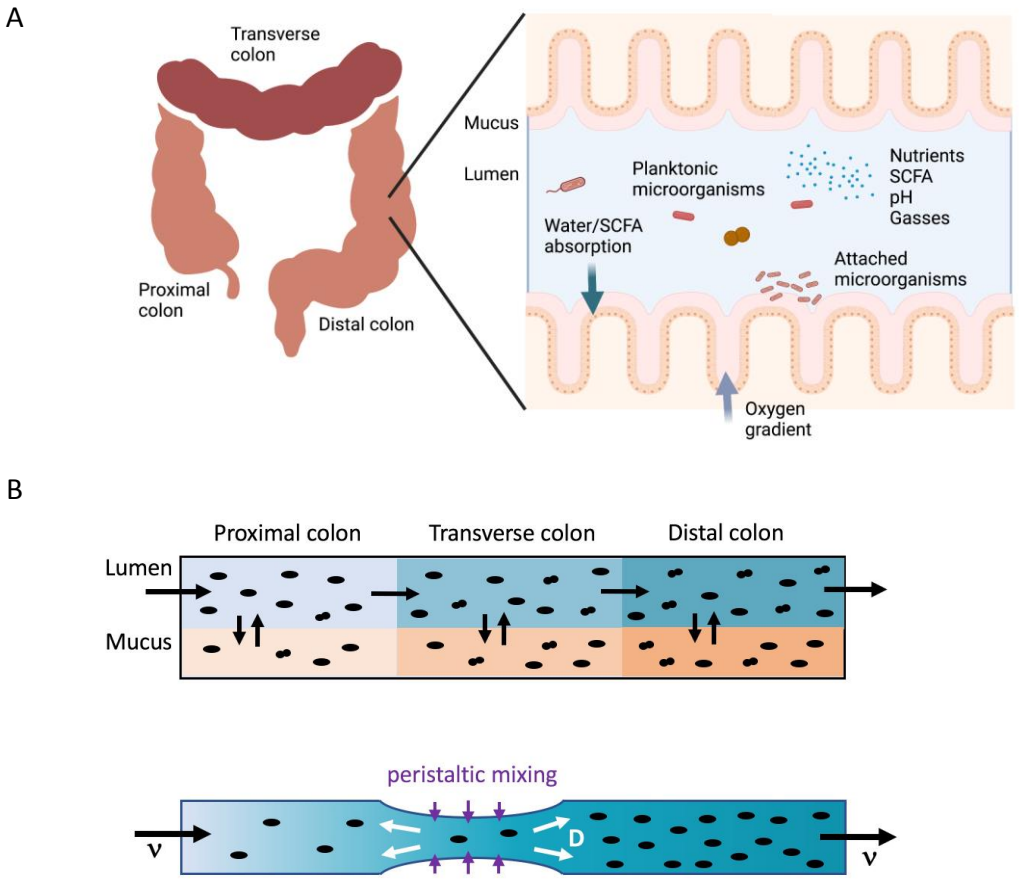

Figure 3: Summary of the components and processes that metabolite-explicit models of human gut microbiota take into account. A) Most spatial models focus on the colon, distinguish between lumen and mucus and account for water absorption, nutrient degradation by gut microbiota and short-chain fatty acid (SCFA) production. A few models also consider oxygen released by epithelial cells and the interplay between metabolites, microorganisms, and pH. Created with BioRender.com. B) The spatial distribution of microbial species and metabolites along the gut can be described by a compartment model consisting of a series of well-mixed bioreactors. Each compartment can be further divided into lumen and mucus. Peristaltic mixing (white arrows) generated by contractions of colonic walls induces a backflow preventing washout due to the continuous flow through the gut (black arrows). When the peristaltic-induced diffusion D is large enough and the flow rate ν not too high, a stable spatial profile of bacterial density (reflected by the blue gradient) can be established.

Metabolite-explicit models of gut microbiota accounting for spatial structure

The model developed by Muñoz-Tamayo and co-authors takes both longitudinal and cross-sectional spatial structure into account by introducing compartments representing the proximal, transverse, and distal colon, each of which is further divided into mucus and lumen. It describes the dynamics of key metabolites such as short-chain fatty acids (SCFAs), glucose and gasses as well as the abundances of four functional groups (glucose consumers, lactate consumers, acetogens and methanogens) with ODEs. The model also accounts for microbial aggregation, for instance on food particles and mucus, and absorption of metabolites (Muñoz-Tamayo et al., 2010). Model predictions agreed with observed ratios of acetate, propionate and butyrate and reproduced the observed

increase in SCFA and gas production with higher levels of fiber (Topping and Clifton, 2001). In addition, the model predicted that microbial aggregation is necessary to reproduce observed high fiber degradation rates and high microbial densities.

Cremer and colleagues investigated the effect of fluid dynamics on microbial densities with a partial differential equation (PDE) model (Cremer et al., 2016). The model predicted that contractions of the intestinal walls leading to peristaltic mixing are essential to prevent microbes to be washed out (Figure 3B). This prediction was confirmed with a fluidic channel ("minigut") that mimicked the effect of peristaltic mixing through membrane valves, thereby demonstrating the importance of peristalsis as a factor shaping gut microbiota. In a next step, the authors modified the model to investigate the role of water absorption and nutrient inflow on the ratio of Firmicutes and Bacteroidetes (now Bacteroidota, (Oren and Garrity, 2021)). The model also included pH as a function of the concentrations of SCFA (Cremer et al., 2017). According to the model, Bacteroidota dominate the gut microbiota at low nutrient inflow and water uptake rates whereas Firmicutes dominate at high inflow and water uptake rates. High water absorption increases SCFA concentrations and thus lowers the pH, thereby giving Firmicutes an advantage over Bacteroidota that grow less well at low pH. The model reproduced the observed enrichment of Firmicutes in fecal samples with low Bristol stool score (indicating low water content) and vice versa of Bacteroidota in samples with high Bristol stool score (Falony* et al., 2016).

Following up on the work of Tamayo et al., Labarthe and colleagues investigated drivers of spatial organization of colon microbiota with a 2-dimensional PDE model that distinguished between proximal, transverse and distal colon as well as mucus and lumen and that considered fluid dynamics (viscosity and flow), peristalsis, absorption of water and SCFA at the mucosal wall and metabolite concentrations (Labarthe et al., 2019). The gut microbial community was again divided into four functional groups, including primary fermenters consuming fiber and mucus, lactate consumers, acetogens and methanogens. The model also accounted for active bacterial motion (swimming). As with the preceding ODE model, the authors were able to reproduce observed microbial densities and SCFA ratios. As expected, the model predicted that a high-fiber diet leads to a peak in microbial activity in the distal colon and higher microbial densities. However, it also predicted higher transit speeds in this case, since fibers accumulating near the epithelial wall reduce water availability. Furthermore, the model underlined the role of the mucus layer in maintaining high microbial densities through mucus-derived metabolites and reduced local flow rates (slowdown zones). The importance of these slowdown zones was illustrated by fluorescently colored mouse gut species observed in situ, which reached higher densities closer to the mucus layer (Welch et al., 2017). Furthermore, the model suggested that active swimming of the bacteria enhances carbohydrate consumption.

The models discussed so far do not take the internal metabolism of microbial cells into account. Recently, van Hoek and Merks employed GEMs within a spatially structured (tube-like) environment to investigate the evolution of cross-feeding (Hoek and Merks, 2017). They created "metabacteria", which combine pathways from different gut bacterial species, and simulated evolution by stepwise deletion and reintroduction of reactions. They found that metabacteria with

initially the same metabolism specialize to take on different metabolic roles and stratify spatially, and that this niche specialization is lost with faster transit time. Thus, faster transit time reduces microbial diversity, which agrees with results from cohort studies (e.g. (Vandeputte et al., 2016)). Chan and coworkers embedded GEMs within a spatial structure to explore the effect of oxygen on the distribution of aerobes and anaerobes in the mucus and lumen of different intestinal sections, which vary in oxygen availability (Chan et al., 2019). They applied SteadyCom, a static FBA tool (Hung et al., 2017), to model microbial metabolism in the mucus and DMMM (Dynamic Multi-species Metabolic Modeling), a form of dynamic FBA (Zhuang et al., 2011), for the changing conditions in the lumen. In their simulated five-species community, *Corynebacterium glutamicum* was only present in luminal and mucosal communities of the small intestine, which agrees with the previous report of its absence in fecal samples (Albenberg et al., 2014). Spatially embedded GEMs are also applied to predict the outcome of perturbations. For example, CODY (COmputing the DYnamics of the gut microbiota) was developed to predict the effects of dietary interventions on gut microbiota (Geng et al., 2021). CODY combines three connected models that represent the gut bacterial metabolism (ECMF), the interactions between gut bacteria (HRAF) and the spatial structure of the gut (SPCF), respectively. To build the ECMF, GEMs of eight bacterial species were simplified by extracting feasible metabolic pathway modules, which were then combined with a regulation layer that allows simulated gut bacteria to switch between pathway modules depending on conditions. The SPCF models the spatial structure of the gut with a series of compartments representing different colon sections as well as lumen and mucus and also accounts for water absorption, microbial detachment, and peristaltic mixing. ECMF and SPCF are connected through the HRAF, which first distributes dietary carbohydrates to species according to their local abundances, and then generates degradation products with the ECMF, accounting for microbial interactions through metabolite exchange. CODY successfully predicts changes in both fecal microbial abundances and plasma metabolite concentrations in two dietary intervention cohorts.

Metabolite-explicit models of gut microbiota without spatial structure

Several metabolite-explicit modeling approaches do not account for spatial structure and instead model the human gut microbiota as a well-stirred system.

Kinetic models are predominantly applied *in vitro*, where it is easier to obtain time series of metabolite concentrations and biomass needed to derive uptake, consumption and growth rates. Kinetic models can have a purely descriptive function, for instance to model the conversion of lactate and acetate to butyrate and bacterial biomass (Muñoz-Tamayo et al., 2011), but they can also be predictive. This was tested for several synthetic gut communities (D'hoe et al., 2018; Pinto et al., 2017; Wey et al., 2014), where a kinetic model parameterized on monocultures predicted community dynamics in two cases. However, this approach failed for a community consisting of *Faecalibacterium prausni*tzii, *Roseburia intestinalis* and *Blautia hydrogenotrophica*, for which data from species pairs were required to reproduce community dynamics (D'hoe et al., 2018). Transcriptomics confirmed that these gut bacteria alter their metabolism in the presence of interaction partners. In addition, community composition and consequently butyrate production depended sensitively on initial conditions.

Going a step further, Kettle and coauthors applied a kinetic model to a complex gut community, i.e. a bioreactor inoculated with a fecal slurry (Kettle et al., 2015). Species were assigned to ten functional groups based on their main substrates and/or products (e.g. lactate producers, acetogens etc.). Each functional group was instantiated with ten strains that took random values for the kinetic parameters within given limits. In a form of parameter screening, the authors then performed 100 simulations to find strain combinations that led to functional group abundances and metabolite concentrations close to those observed in the bioreactor. The authors then simulated perturbations and compared resulting biomass and metabolite concentrations to the experimental data. For instance, they found that Bacteroides dominates the community at high (6.5) pH, but not at lower (5.5) pH. They also predicted that omitting the functional group of Bacteroides results in an increase in butyrate. In addition, when decreasing the number of strains per functional group, the variability of strain abundances and metabolite concentrations increased, which is interesting since disease-associated gut communities often have fewer species (Mosca et al., 2016) and are more variable (Zaneveld et al., 2017) than healthy ones. In a next step, Wang and colleagues applied the kinetic model of Kettle and colleagues to interpret observations in continuous bioreactors seeded with fecal slurries from different donors and supplied with lactate (Wang et al., 2020). To reproduce experimental findings, the model needed to be extended with an inhibitory effect of lactate on all functional groups except lactate producers. This growth inhibition was confirmed experimentally for several gut bacterial species in monoculture at low (5.5) pH and suggests an important role of lactate producers and consumers in the human gut ecosystem.

Wang and colleagues rely on the combination of several consumer-resource models, each one specific to a "trophic level", to model complex gut microbial communities (Wang et al., 2019). The trophic levels correspond to primary, secondary, and tertiary fermentation, where polysaccharides are first degraded to monosaccharides and acids, which are then converted by secondary fermenters to SCFAs. Acetogens, sulfate-reducing bacteria and methanogens, which grow on the byproducts of secondary fermenters, are considered as tertiary fermenters. The species-metabolite matrices for each level were taken from a gut microbial interaction network compiled from the literature (Sung et al., 2017), and a number of simplifying assumptions were made to fill in uptake and consumption rates. Each level produces metabolites that are fed to the next level, but metabolites and species can appear on more than one level. The trophic model requires microbial abundances derived from sequencing data to know which species are present in each level and then predicts the metabolites that remain after nutrients have passed through several levels. After having varied the number of trophic levels in the model, the authors concluded that four such levels lead to the best agreement of predicted metabolites with fecal metabolomics data.

In contrast to kinetic models, metabolic models do not require parameters when assuming steady-state conditions, but they often require abundance data to compute flux distributions in the community. Metabolic models have been applied to data from several disease cohorts to link changes in metabolite profiles to gut microbial species. For instance, the Microbiome Modeling Toolbox was employed to construct metabolic community models for 31 Parkinson's patients and 28 matched controls (Hertel et al., 2019), using the AGORA collection of metabolic reconstructions of human gut bacteria (Magnúsdóttir et al., 2017). These models predicted an overrepresentation of

sulfur metabolites in Parkinson's disease, which was matched by an observed increase in metabolites involved in the transsulfuration pathway. Transsulfuration is involved in the production of taurine-conjugated bile acids, which are associated with lower disease risk. In the metabolic models, *Akkermansia muciniphila* and *Bilophila wadsworthia* were significant contributors to hydrogen sulfide and sulfite secretion, respectively. Based on these results, Hertel and colleagues proposed that gut bacteria remove taurine from conjugated bile acids, thereby modulating the severity of Parkinson's disease. In another example, Garza and coworkers used metabolomics data from colorectal cancer (CRC) patients to identify gut bacteria that have a growth advantage in CRC patients (Garza et al., 2020). For this, a basal gut medium was first derived from stool metagenomes with MAMBO (Garza et al., 2018) and 29 metabolites enriched in CRC were removed one by one from this medium to explore their effect on growth *in silico*. The growth of bacterial genera observed to be enriched in CRC was predicted to be significantly affected by the removal of CRC metabolites but not of random metabolites. Thus, metabolic models helped to unravel mechanisms connecting gut microbiota to diseases.

What are the challenges of metabolite-explicit models?

Metabolic models require the construction of GEMs, which comes with several challenges. Many-to-many relationships between genes and functions (e.g. isoenzymes and multifunctional enzymes) make it hard to identify the correct set of genome-encoded reactions. For GEMs to accurately recapitulate microbial metabolism and predict growth rates, the chemical composition of the environment (medium) needs to be known and the biomass reaction needs to reflect the cell's composition correctly. Obtaining such measurements is work-intensive and not possible for uncultured microbes. In addition, the assumption that evolution has led to the maximization of growth rates may not always be true (Segrè et al., 2002). For example, some cells may invest in slower growth but higher yield (Wortel et al., 2018). Furthermore, environmental factors such as pH or osmotic pressure are difficult to account for in GEMs (Bernstein et al., 2021). In communities, objective functions are particularly challenging to define. Optimizing the objective function of each species independently from the others is not suited for mutualistic relationships, where partners have co-evolved to optimize a combined metabolic network, or for instances of group selection e.g. in host-associated communities. Strategies that jointly optimize objective functions of different species handle these cases better, but they do so at the cost of being unable to accurately describe exploitative relationships, where a species grows at the expense of another even if that lowers the overall biomass. As we have seen, some tools circumvent this dilemma by optimizing the objective function to reproduce observed species abundances, but that also means that they can no longer predict community composition for a given set of species. Contrary to FBA, flux sampling does not depend on an objective function. However, the distribution of fluxes during microbial growth is the result of evolutionary processes, which may not be accurately predicted from uniformly sampling the flux space of the stoichiometric matrix. Nevertheless, working with flux distributions instead of a single solution accounts better for the observed variability of fluxes (Wintermute et al., 2013) and novel methods may be devised to obtain flux distributions that accurately reflect experimental data (Martino et al., 2018). Finally, FBA and flux sampling approaches can only model metabolite-mediated ecological interactions. They are not designed to handle interference competition through

direct killing mechanisms (such as Type VI secretion systems) or to model exploitation, where one organism consumes or parasitizes another. Thus, metabolic models do not cover the whole range of ecological interactions.

Kinetic models avoid the challenges posed by GEM construction and objective functions and make it easier to include ecological interactions that are not mediated by metabolites. However, they require more system knowledge in the form of kinetic parameters and equation structure. Furthermore, the equations are often over-simplistic and may not generalize when conditions change. For example, based on monoculture experiments (Porter and Larsbrink, 2022), a kinetic model could represent a Bacteroides species with equations for carbohydrate consumption and production of a number of fermentation products such as acetate, lactate, succinate, and formate. However, its metabolic network suggests that an external supply of CO_2 would allow Bacteroides to reduce more fumarate to succinate (Fischbach and Sonnenburg, 2011), so that it no longer needs to produce lactate. If other bacteria depend on lactate as energy source, then CO_2 would change the dynamics. It is an open question how to take advantage of the knowledge encoded in the metabolic network without the unrealistic assumptions introduced by FBA. One approach is coarse-graining the metabolic network into a much smaller set of key reactions, which retain the metabolic flexibility of the system and can still fit the available experimental data. The system can be described and simulated by a set of deterministic or stochastic ODEs. For a first approximation, one may focus on the central carbon and energy pathways, collapsing linear pathways into single equations while retaining their substrates and products. We illustrate this on a coarse-grained approximation to the toy model illustrated in Box 1 (Supplementary Figure 2).
Both kinetic and metabolic models can describe heterogeneity on the population level through individual-based modeling, which is for instance implemented in GutLogo (Lin et al., 2018) and BacArena (Bauer et al., 2017). In contrast to metabolic models, kinetic or coarse-grained models can also be implemented as stochastic models that account for molecular noise (Lecca, 2013) as shown in the example (Supplementary Figure 2).

Metabolite-explicit community models are challenging to validate comprehensively. It is straightforward to compare predictions of fecal microbial composition and metabolite concentrations to measurements. However, species abundances predicted for different colon segments or the effect of the removal of a functional group are harder to confirm. The hardest predictions to test are those of species-specific uptake and consumption rates as well as internal fluxes in a community context. Kinetic parameters are usually obtained from measurements in monoculture and may change in a community. Although metatranscriptomics indicates which pathways are active in which species, enzyme expression levels are not equivalent to fluxes and do not provide uptake or consumption rates. Although reaction rates can be measured at the community level (e.g. acetogenesis), resolving each species' contribution to these rates is one of the great challenges in microbial ecology. Advances in single-cell technologies, in particular Raman microspectroscopy (Hatzenpichler et al., 2020), offer new tools to tackle this problem. For instance, Chisanga and colleagues were able to derive the kinetics of substrate uptake in *Escherichia coli* with both Raman and Fourier-transform infrared spectroscopy by measuring spectral shifts in single cells *in vivo* (Chisanga et al., 2021). It may be possible to extend this approach to communities.

When validation data are scarce, there is a risk of overfitting. It is of note that despite their substantial differences in assumptions and structure, several models were able to predict metabolite concentrations in fecal samples. This may be due to overfitting, which would imply that the structure of these models is not as informative as we hope it to be. A model with many parameters increases the risk of overfitting, and thus the complexity of a metabolic model should be adapted both to its purpose and the available data. In the absence of sufficient data, a black-box approach to the prediction of fecal metabolites from sequencing data such as MelonnPan (Mallick et al., 2019) may be more appropriate than a complex metabolic model with a large number of untested assumptions. If species identity is not important to the research question, then models aggregating species by function or phylogeny are a good way to reduce complexity. However, the successful use of a therapeutic consortium may sensitively depend on the abundances of particular species being present, and thus in clinical applications, a species-level metabolic model may be necessary.

It is an open question whether metabolic models can generate the complex dynamics that is occasionally observed experimentally, such as multi-stability (Khazaei et al., 2020), oscillations or chaos (Beck et al., 2018). The stable marriage model integrates metabolic information in an original manner by considering a matrix of metabolite preferences per microorganism and a matrix of microorganisms ranked by their consumption rate per metabolite. Given these rankings, the model identifies stable pairs ("marriages") of microbes and metabolites (Goyal et al., 2018). This model was applied to seven Bacteroides species growing on nine polysaccharides. Interestingly, the authors found species sub-sets giving up to five different stable states and thus the stable marriage model can easily generate multi-stability. If a microbial community displays complex behavior, metabolic community models assuming steady state conditions are not suitable. However, dynamic FBA can reproduce such behavior. For instance, bistability occurred in simulations with a dynamic FBA model of a two-species system (*Bacteroides thetaiotaomicron* and *Klebsiella pneumoniae*) and was confirmed experimentally (Khazaei et al., 2020). It remains to be seen whether other complex dynamics, e.g. oscillations in gut microbiota linked to circadian rhythms (Rosselot et al., 2016), can be reproduced with metabolic models.

Finally, even the most complex metabolite-explicit models discussed here omit a number of biological components known to be relevant *in vivo*, such as the immune system, which interacts with gut microorganisms e.g. through antimicrobial peptides and antibodies (Zheng et al., 2020), or the role of gut bacteriophages (Sausset et al., 2020). Extending models to take these factors into account is a further challenge.

In conclusion, several metabolite-explicit models have been developed that account for a number of phenomena shaping human gut microbiota, which led to interesting biological hypotheses and findings. However, these models still face challenges concerning construction, parameterization and validation that represent exciting topics for future research.

Supplementary Figure 1: Metabolic networks of the toy species. (A) A carbohydrate fermenter (for example, a primary fermenter such as Bacteroides species that feed on sugars (here only glucose represented) and can secrete succinate, lactate, acetate, and formate; (B) A butyrate producer that can use sugars, lactate, and acetate and secretes butyrate, CO_2, and H_2. (C) An acetogen that due to the presence of the Wood Ljungdahl pathway (WL) can either grow in a combination of CO_2/formate and H_2 as a lithotroph or feed on sugars. In both cases it secretes acetate.

Supplementary Figure 2: Stochastic course-grained model. Reactions from linear pathways of the toy model (Box 1) were merged into representative coarse-grained reactions (Supplementary Table 3). Each reaction has a probability of occurring in time, which is derived from the product of reaction rates and the number of distinct reaction substrate combinations. The stochastic trajectories displayed in the insets are the average of ten independent simulations. The temporal dynamics of the system exhibit properties that depend on metabolism alone and are not deducible from the metabolic network. For instance, lactate is first produced then consumed, while formate is continuously produced and consumed in small amounts due the limiting amount of H_2. Starting from 10 units of sugar, the system accumulates succinate, formate, acetate, CO_2, and butyrate. Also, the metabolite trajectories in the carbohydrate fermenter vary little between independent simulations (are deterministic), while they exhibit noisy trajectories in the other species. Biologically, this could mean that the carbohydrate fermenter can harvest energy from glucose with minimal need for regulation, but once glucose is depleted, no further metabolic activity takes place. This observation is also consistent with the results of flux sampling (Box 1, Fig. F). Such coarse-grained systems have limited scope as they depend on the previous knowledge of reaction rates but for a small system, where one may manually or systematically try different rates, they may guide the parametrization of the kinetic and dFBA models.

Supplementary Table 1. Parameters of the kinetic model presented in Box 1 and their units.

Supplementary Table 2. Metabolic reactions of the toy model species.

Supplementary Table 3. Reactions of the coarse-grained stochastic kinetic model and arbitrary rates used in the simulations of Supplementary Figure 2.

Acknowledgements

This work was supported by funding from the European Research Council (ERC) under the European Union's Horizon 2020 research and innovation program under grant agreement no. 801747.

References

Albenberg, L., Esipova, T.V., Judge, C.P., Bittinger, K., Chen, J., Laughlin, A., Grunberg, S., Baldassano, R.N., Lewis, J.D., Li, H.*, et al.* (2014). Correlation between intraluminal oxygen gradient and radial partitioning of intestinal microbiota. Gastroenterology *147*, 1055-1063.

Baldini, F., Heinken, A., Heirendt, L., Magnusdottir, S., Fleming, R.M.T., and Thiele, I. (2019). The Microbiome Modeling Toolbox: from microbial interactions to personalized microbial communities. Bioinformatics *35*, 2332-2334.

Bashan, A., Gibson, T.E., Friedman, J., Carey, V.J., Weiss, S.T., Hohmann, E.L., and Liu, Y.-Y. (2016). Universality of human microbial dynamics. Nature *534*, 259-262.

Bauer, E., and Thiele, I. (2018). From metagenomic data to personalized in silico microbiotas: predicting dietary supplements for Crohn's disease. npj Systems Biology and Applications *4*, 27.

Bauer, E., Zimmermann, J., Baldini, F., Thiele, I., and Kaleta, C. (2017). BacArena: Individual-based metabolic modeling of heterogeneous microbes in complex communities. PLoS Computational Biology *13*, e1005544.

Beck, A.E., Hunt, K.A., and Carlson, R.P. (2018). Measuring Cellular Biomass Composition for Computational Biology Applications. Processes *6*, 38.

Belcour, A., Frioux, C., Aite, M., Bretaudeau, A., Hildebrand, F., and Siegel, A. (2020). Metage2Metabo, microbiota-scale metabolic complementarity for the identification of key species. eLife *9*, e61968.

Bernstein, D.B., Sulheim, S., Almaas, E., and Segrè, D. (2021). Addressing uncertainty in genome-scale metabolic model reconstruction and analysis. Genome Biology *22*, 64.

Budinich, M., Bourdon, J., Larhlimi, A., and Eveillard, D. (2017). A multi-objective constraint-based approach for modeling genome-scale microbial ecosystems. PLoS ONE *12*, e0171744.

Butler, S., and O'Dwyer, J.P. (2018). Stability criteria for complex microbial communities. Nature Communications *9*, 2970.

Chan, S.H.J., Friedman, E.S., Wu, G.D., and Maranas, C.D. (2019). Predicting the Longitudinally and Radially Varying Gut Microbiota Composition using Multi-Scale Microbial Metabolic Modeling. Processes *7*, 394.

Chisanga, M., Muhamadali, H., McDougall, D., Xu, Y., Lockyer, N., and Goodacre, R. (2021). Metabolism in action: stable isotope probing using vibrational spectroscopy and SIMS reveals kinetic and metabolic flux of key substrates. Analyst *146*, 1734.

Coyte, K.Z., Schluter, J., and Foster, K.R. (2015). The ecology of the microbiome: Networks, competition, and stability. Science *350*, 663-666.

Cremer, J., Arnoldini, M., and Hwa, T. (2017). Effect of water flow and chemical environment on microbiota growth and composition in the human colon. PNAS *114*, 6438-6443.

Cremer, J., Segota, I., Yang, C.-y., Arnoldini, M., Sauls, J.T., Zhang, Z., Gutierrez, E., Groisman, A., and Hwa, T. (2016). Effect of flow and peristaltic mixing on bacterial growth in a gut-like channel. PNAS *113*, 11414-11419.

D'hoe, K., Vet, S., Faust, K., Moens, F., Falony, G., Gonze, D., Lloréns-Rico, V., Gelens, L., Danckaert, J., Vuyst, L.D*., et al.* (2018). Integrated culturing, modeling and transcriptomics uncovers complex interactions and emergent behavior in a three-species synthetic gut community. eLife *7*, e37090.

Diener, C., Gibbons, S.M., and Resendis-Antonio, O. (2020). MICOM: Metagenome-Scale Modeling To Infer Metabolic Interactions in the Gut Microbiota. mSystems *5*, e00606-00619.

Donaldson, G.P., Lee, S.M., and Mazmanian, S.K. (2016). Gut biogeography of the bacterial microbiota. Nature Reviews Microbiology *14*, 20-32.

Dukovski, I., Bajić, D., Chacón, J.M., Quintin, M., Vila, J.C.C., Sulheim, S., Pachec, A.R., Bernstein, D.B., Riehl, W.J., Korolev, K.S*., et al.* (2021). A metabolic modeling platform for the computation of microbial ecosystems in time and space (COMETS). Nature protocols *16*, 5030-5082.

Enjalbert, B., Cocaign-Bousquet, M., Portais, J., and Letisse, F. (2015). Acetate exposure determines the diauxic behavior of Escherichia coli during the glucose-acetate transition. J Bacteriology *197*, 3173–3181.

Falony*, G., Joossens*, M., Vieira-Silva*, S., Wang*, J., Darzi, Y., Faust, K., Kurilshikov, A., Bonder, M.J., Valles-Colomer, M., Vandeputte, D*., et al.* (2016). Population-level analysis of gut microbiome variation. Science *352*, 560-564.

Fischbach, M.A., and Sonnenburg, J.L. (2011). Eating for two: how metabolism establishes interspecies interactions in the gut. Cell Host Microbe *10*, 336-347.
Garza, D.R., Taddese, R., Wirbel, J., Zeller, G., Boleij, A., Huynen, M.A., and Dutilh, B.E. (2020). Metabolic models predict bacterial passengers in colorectal cancer. Cancer & Metabolism *8*.
Garza, D.R., Verk, M.C.v., Huynen, M.A., and Dutilh, B.E. (2018). Towards predicting the environmental metabolome from metagenomics with a mechanistic model. Nature Microbiology *3*, 456-460.
Geng, J., Ji, B., Li, G., López-Isunza, F., and Nielsen, J. (2021). CODY enables quantitatively spatiotemporal predictions on in vivo gut microbial variability induced by diet intervention. PNAS *118*, e2019336118.
Goyal, A., Dubinkina, V., and Maslov, S. (2018). Multiple stable states in microbial communities explained by the stable marriage problem. The ISME Journal *12*, 2823-2834.
Haraldsdóttir, H.S., Cousins, B., Thiele, I., Fleming, R.M.T., and Vempala, S. (2017). CHRR: coordinate hit-and-run with rounding for uniform sampling of constraint-based models. Bioinformatics *33*, 1741-1743.
Hatzenpichler, R., Krukenberg, V., Spietz, R.L., and Jay, Z.J. (2020). Next-generation physiology approaches to study microbiome function at single cell level. Nature Reviews Microbiology *18*, 241-256.
Heinken, A., Basile, A., and Thiele, I. (2021). Advances in constraint-based modelling of microbial communities. Current Opinion in Systems Biology *27*, 100346.
Heinken, A., Sahoo, S., Fleming, R.M.T., and Thiele, I. (2013). Systems-level characterization of a host-microbe metabolic symbiosis in the mammalian gut. Gut Microbes *4*, 28-40.
Henson, M.A., and Hanly, T.J. (2014). Dynamic flux balance analysis for synthetic microbial communities. IET Systems Biology *8*, 214-229.
Herrmann, H.A., Dyson, B.C., Vass, L., Johnson, G.N., and Schwartz, J.-M. (2019). Flux sampling is a powerful tool to study metabolism under changing environmental conditions. npj Systems Biology and Applications *5*, 32.
Hertel, J., Harms, A.C., Heinken, A., Baldini, F., Thinne, C.C., Glaab, E., Vasco, D.A., Pietzner, M., Stewart, I.D., Wareham, N.J.*, et al.* (2019). Integrated Analyses of Microbiome and Longitudinal Metabolome Data Reveal Microbial-Host Interactions on Sulfur Metabolism in Parkinson's Disease. Cell Reports *29*, 1767-1777.
Hoek, M.J.A.v., and Merks, R.M.H. (2017). Emergence of microbial diversity due to cross-feeding interactions in a spatial model of gut microbial metabolism. BMC Systems Biology *11*, 56.
Hung, S., Chan, J., Simons, M.N., and Maranas, C.D. (2017). SteadyCom: Predicting microbial abundances while ensuring community stability. PLoS Computational Biology *13*, e1005539.
Kettle, H., Holtrop, G., Louis, P., and Flint, H.J. (2018). microPop: Modelling microbial populations and communities in R. Methods in Ecology and Evolution *9*, 399-409.
Kettle, H., Louis, P., Holtrop, G., Duncan, S.H., and Flint, H.J. (2015). Modelling the emergent dynamics and major metabolites of the human colonic microbiota. Environmental Microbiology *17*, 1615-1630.
Khazaei, T., Williams, R.L., Bogatyrev, S.R., Doyle, J.C., Henry, C.S., and Ismagilov, R.F. (2020). Metabolic multistability and hysteresis in a model aerobe-anaerobe microbiome community. Science Advances *6*, eaba0353.
Kreimer, A., Doron-Faigenboim, A., Borenstein, E., and Freilich, S. (2012). NetCmpt: a network-based tool for calculating the metabolic competition between bacterial species. Bioinformatics *28*, 2195-2197.
Labarthe, S., Polizzi, B., Phan, T., Goudon, T., Ribot, M., and Laroche, B. (2019). A mathematical model to investigate the key drivers of the biogeography of the colon microbiota. Journal of Theoretical Biology *462*, 552-581.
Lecca, P. (2013). Stochastic chemical kinetics : A review of the modelling and simulation approaches. Biophysical Review *5*, 323-345.
Levy, R., and Borenstein, E. (2013). Metabolic modeling of species interaction in the human microbiome elucidates community-level assembly rules. Proceedings of the National Academy of Sciences *110*, 12804-12809.

Levy, R., Carr, R., Kreimer, A., Freilich, S., and Borenstein, E. (2015). NetCooperate: a network-based tool for inferring host-microbe and microbe-microbe cooperation. BMC Bioinformatics *16*, 164.
Lin, C., Culver, J., Weston, B., Underhill, E., Gorky, J., and Dhurjati, P. (2018). GutLogo: Agent-based modeling framework to investigate spatial and temporal dynamics in the gut microbiome. PLOS ONE *13*, e0207072.
Lotka, A.J. (1925). Elements of physical biology. (Williams and Wilkins).
Louis, P., Hold, G.L., and Flint, H.J. (2014). The gut microbiota, bacterial metabolites and colorectal cancer. Nature Reviews Microbiology *12*, 661-672.
MacArthur, R.H. (1970). Species packing and competitive equilibria for many species. Theoretical Population Biology *1*, 1-11.
Magnúsdóttir, S., Heinken, A., Kutt, L., Ravcheev, D.A., Bauer, E., Noronha, A., Greenhalgh, K., Jäger, C., Baginska, J., Wilmes, P.*, et al.* (2017). Generation of genome-scale metabolic reconstructions for 773 members of the human gut microbiota. Nature Biotechnology *35*, 81-89.
Mahadevan, R., Edwards, J.S., and 3rd, F.J.D. (2002). Dynamic flux balance analysis of diauxic growth in Escherichia coli. Biophysical Journal *83*, 1331-1340.
Mallick, H., Franzosa, E.A., Mclver, L.J., Banerjee, S., Sirota-Madi, A., Kostic, A.D., Clish, C.B., Vlamakis, H., Xavier, R.J., and Huttenhower, C. (2019). Predictive metabolomic profiling of microbial communities using amplicon or metagenomic sequences. Nature Communications *10*, 3136.
Marsland, R., Cui, W., Goldford, J., and Mehta, P. (2020). The Community Simulator: A Python package for microbial ecology. PLOS ONE *15*, e0230430.
Martino, D.D., Andersson, A.M., Bergmiller, T., Guet, C.C., and Tkačik, G. (2018). Statistical mechanics for metabolic networks during steady state growth. Nature Communications *9*, 2988.
May, R.M. (1972). Will a large complex system be stable? Nature *238*, 413-414.
Megchelenbrink, W., Huynen, M., and Marchiori, E. (2014). optGpSampler: an improved tool for uniformly sampling the solution-space of genome-scale metabolic networks. PLoS ONE *9*, e86587.
Momeni, B., Xie, L., and Shou, W. (2017). Lotka-Volterra pairwise modeling fails to capture diverse pairwise microbial interactions. eLIFE *6*, e25051.
Monod, J. (1949). The growth of bacterial cultures. Annual Review of Microbiology *3*, 371-394.
Mosca, A., MarionLeclerc, and Hugot, J.P. (2016). Gut Microbiota Diversity and Human Diseases: Should We Reintroduce Key Predators in Our Ecosystem? Frontiers in Microbiology *7*, 455.
Muñoz-Tamayo, R., Laroche, B., Walter, É., Doré, J., Duncan, S.H., J.Flint, H., and Leclerc, M. (2011). Kinetic modelling of lactate utilization and butyrate production by key human colonic bacterial species. FEMS Microbiology Ecology *76*, 615-624.
Muñoz-Tamayo, R., Laroche, B., Walter, É., Doré, J., and MarionLeclerc (2010). Mathematical modelling of carbohydrate degradation by human colonic microbiota. Journal of Theoretical Biology *266*, 189-201.
Niehaus, L., Boland, I., Liu, M., Chen, K., Fu, D., Henckel, C., Chaung, K., Miranda, S.E., Dyckman, S., Crum, M.*, et al.* (2019). Microbial coexistence through chemical-mediated interactions. Nature Communications *10*, 2052.
Oren, A., and Garrity, G.M. (2021). Valid publication of the names of forty-two phyla of prokaryotes. INTERNATIONAL JOURNAL OF SYSTEMATIC AND EVOLUTIONARY MICROBIOLOGY *71*, 005056.
Pinto, F., Medina, D.A., Pérez-Correa, J.R., and Garrido, D. (2017). Modeling Metabolic Interactions in a Consortium of the Infant Gut Microbiome. Frontiers in Microbiology *8*, 2507.
Popp, D., and Centler, F. (2020). µBialSim: Constraint-Based Dynamic Simulation of Complex Microbiomes. Frontiers in Bioengineering and Biotechnology *8*, 574.
Porter, N.T., and Larsbrink, J. (2022). Investigation and Alteration of Organic Acid Synthesis Pathways in the Mammalian Gut Symbiont Bacteroides thetaiotaomicron. Microbiology Spectrum *10*, e02312-02321.
Rosselot, A.E., Hong, C.I., and Moore, S.R. (2016). Rhythm and bugs: Circadian clocks, gut microbiota, and enteric infections. Current Opinion Gastroenterology *32*, 7-11.

Sausset, R., Petit, M.A., Gaboriau-Routhiau, V., and Paepe, M.D. (2020). New insights into intestinal phages. Mucosal Immunology *13*, 205-215.
Sauvaitre, T., Etienne-Mesmin, L., Sivignon, A., Mosoni, P., Courtin, C.M., Wiele, T.V.d., and Blanquet-Diot, S. (2021). Tripartite relationship between gut microbiota, intestinal mucus and dietary fibers: towards preventive strategies against enteric infections. FEMS Microbiology Reviews *45*, fuaa052.
Schellenberger, J., and Palsson, B.Ø. (2009). Use of Randomized Sampling for Analysis of Metabolic Networks. Journal of Biological Chemistry *284*, 5457-5461.
Schmidt, J., Riedele, C., Regestein, L., Rausenberger, J., and Reichl, U. (2011). A novel concept combining experimental and mathematical analysis for the identification of unknown interspecies effects in a mixed culture. Biotechnology and Bioengineering *108*, 1900-1911.
Seaver, S.M.D., Liu, F., Zhang, Q., Jeffryes, J., Faria, J.P., Edirisinghe, J.N., Mundy, M., Chia, N., Noor, E., Beber, M.E*., et al.* (2021). The ModelSEED Biochemistry Database for the integration of metabolic annotations and the reconstruction, comparison and analysis of metabolic models for plants, fungi and microbes. Nucleic Acids Research *49*, D575-D588.
Segrè, D., Vitkup, D., and Church, G.M. (2002). Analysis of optimality in natural and perturbed metabolic networks. PNAS *99*, 15112-15117.
Shoaie, S., Ghaffari, P., Kovatcheva-Datchary, P., Mardinoglu, A., Sen, P., Pujos-Guillot, E., Wouters, T.d., Juste, C., Rizkalla, S., Chilloux, J*., et al.* (2015). Quantifying Diet-Induced Metabolic Changes of the Human Gut Microbiome. Cell Metabolism *22*, 320-331.
Smith, N.W., Shorten, P.R., Altermann, E., Roy, N.C., and McNabb, W.C. (2021). Examination of hydrogen cross-feeders using a colonic microbiota model. BMC Bioinformatics *22*, 3.
Stolyar, S., Dien, S.V., Hillesland, K.L., Pinel, N., Lie, T.J., Leigh, J.A., and Stahl, D.A. (2007). Metabolic modeling of a mutualistic microbial community. Molecular Systems Biology *3*, 92.
Sung, J., Kim, S., Cabatbat, J.J.T., Jang, S., Jin, Y.-S., Jung, G.Y., Chia, N., and Kim, P.-J. (2017). Global metabolic interaction network of the human gut microbiota for context-specific community-scale analysis. Nature Communications *8*, 15393.
Thiele, I., and Palsson, B.Ø. (2010). A protocol for generating a high-quality genome-scale metabolic reconstruction. Nature Protocols *5*, 93-121.
Topping, D.L., and Clifton, P.M. (2001). Short-chain fatty acids and human colonic function: roles of resistant starch and nonstarch polysaccharides. Physiol Rev *81*, 1031-1064.
Tropini, C., Earle, K.A., Huang, K.C., and Sonnenburg, J.L. (2017). The Gut Microbiome: Connecting Spatial Organization to Function. Cell Host Microbe *21*, 433-442.
Vandeputte, D., Falony, G., Vieira-Silva, S., Tito, R.Y., Joossens, M., and Raes, J. (2016). Stool consistency is strongly associated with gut microbiota richness and composition, enterotypes and bacterial growth rates Gut *65*, 57-62.
Volterra, V. (1926). Fluctuations in the abundance of a species considered mathematically. Nature *118*, 558-560.
Wang, S.P., Rubio, L.A., Duncan, S.H., Donachie, G.E., Holtrop, G., Lo, G., Farquharson, F.M., Wagner, J., Parkhill, J., Louis, P*., et al.* (2020). Pivotal Roles for pH, Lactate, and Lactate-Utilizing Bacteria in the Stability of a Human Colonic Microbial Ecosystem. mSystems *5*, e00645-00620.
Wang, T., Goyal, A., Dubinkina, V., and Maslov, S. (2019). Evidence for a multi-level trophic organization of the human gut microbiome. PLoS Computational Biology *15*, e1007524.
Welch, J.L.M., Hasegawa, Y., McNulty, N.P., Gordon, J.I., and Borisy, G.G. (2017). Spatial organization of a model 15-member human gut microbiota established in gnotobiotic mice. PNAS *114*, E9105-E9114.
Wey, A.S.V., Cookson, A.L., Roy, N.C., McNabb, W.C., Soboleva, T.K., and Shorten, P.R. (2014). Monoculture parameters successfully predict coculture growth kinetics of Bacteroides thetaiotaomicron and two Bifidobacterium strains. Int J Food Microbiol *191*, 172-181.

Wintermute, E.H., Lieberman, T.D., and Silver, P.A. (2013). An objective function exploiting suboptimal solutions in metabolic networks. BMC Systems Biology *7*, 98.
Wortel, M.T., Noor, E., Ferris, M., Bruggeman, F.J., and Liebermeister, W. (2018). Metabolic enzyme cost explains variable trade-offs between microbial growth rate and yield. PLoS Computational Biology *14*, e1006010.
Zaneveld, J.R., McMinds, R., and Thurber, R.V. (2017). Stress and stability: applying the Anna Karenina principle to animal microbiomes. Nature Microbiology *2*, 1721.
Zhang, Z., Geng, J., Tang, X., Fan, H., Xu, J., Wen, X., Ma, Z.S., and Shi, P. (2014). Spatial heterogeneity and co-occurrence patterns of human mucosal-associated intestinal microbiota. The ISME Journal *8*, 881-893.
Zheng, D., Liwinski, T., and Elinav, E. (2020). Interaction between microbiota and immunity in health and disease. Cell Research *30*, 492-506.
Zhuang, K., Izallalen, M., Mouser, P., Richter, H., Risso, C., Mahadevan, R., and Lovley, D. (2011). Genome-scale dynamic modeling of the competition between Rhodoferax and Geobacter in anoxic subsurface environments. ISME Journal *5*, 305-316.

Supplementary Figure 1

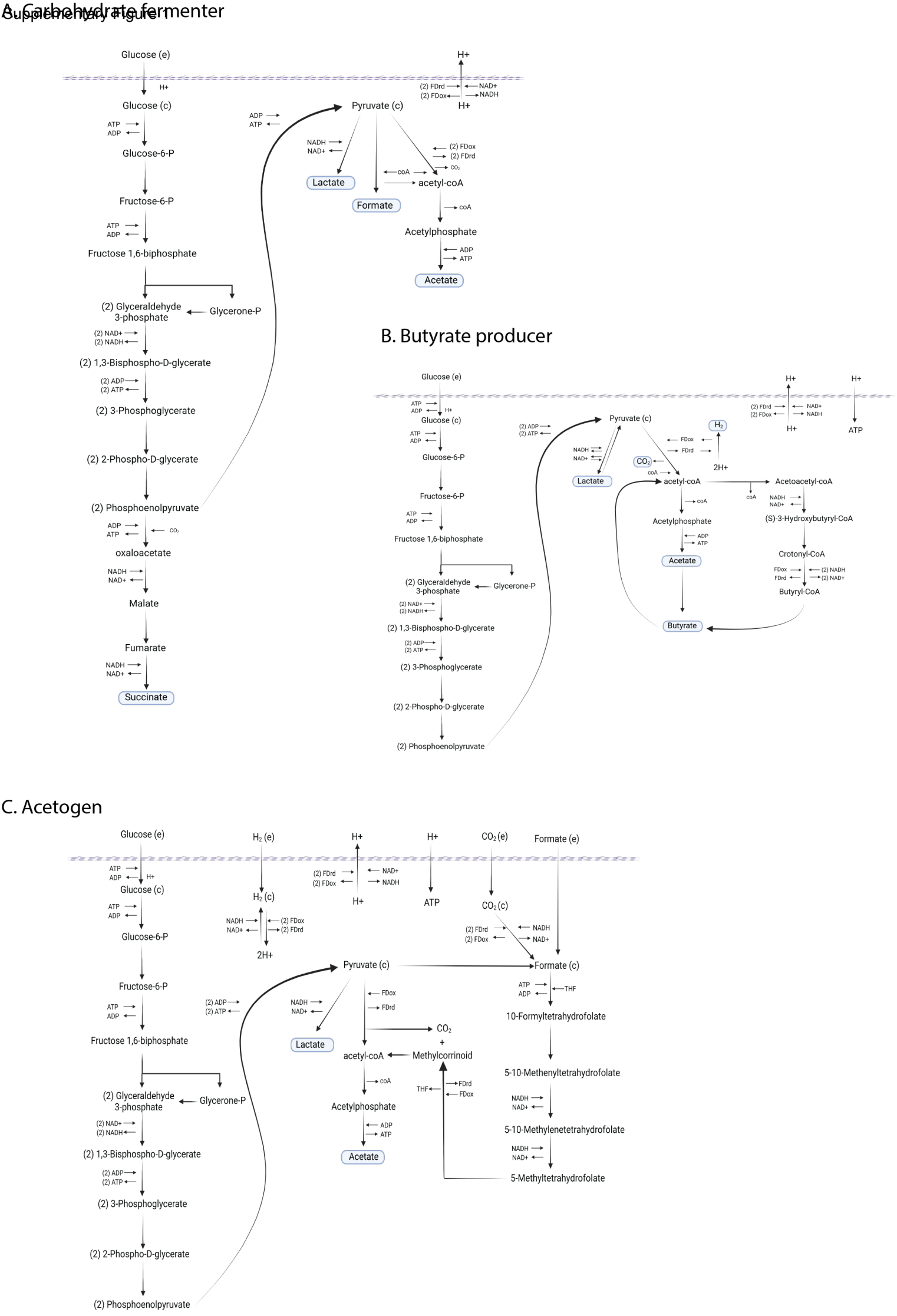

Supplementary Figure 2

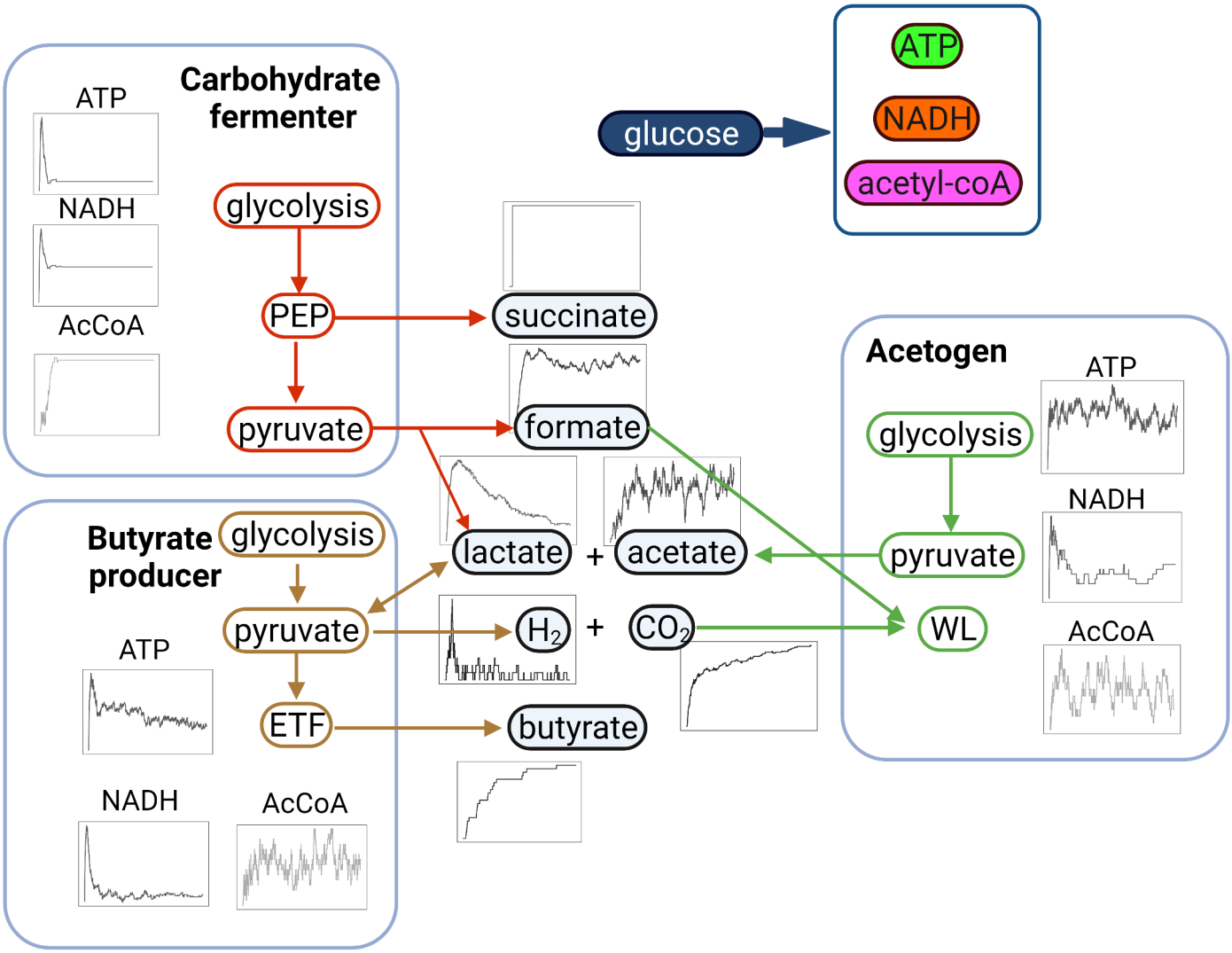

Supplementary Table 1

Variables	Description	Initial value
C	Biomass of Carbohydrate fermenter (C)	0.1
B	Biomass of Butyrate producer (B)	0.1
A	Biomass of Acetogen (A)	0.1
Glu	Concentration of glucose	0
Ac	Concentration of acetate	0
For	Concentration of formate	0
$C0_2$	Concentration of C02	0
Parameter	**Description**	**Value**
φ	Flow rate	0.1
Glu_{in}	Concentration of supplied glucose	8
μ_{max1}	Growth rate of Carbohydrate fermenter (C)	1.1
μ_{max2}	Growth rate of Butyrate producer (B)	0.6
μ_{max3}	Growth rate of Acetogen (A)	1
$K_{11}=K_{21}=K_{22}=K_{31}=K_{33}=K_{34}$	Monod constants	1
$Y_{11}=Y_{21}=Y_{31}=Y_{22}=Y_{33}=Y_{34}$	Yields	1
$w_{22}=w_{33}=w_{34}$	Weights	1
$\alpha_{12}=\alpha_{32}=\alpha_{13}=\alpha_{24}$	Metabolite production rates	1

Tentative units
mmol gDW
mmol gDW
mmol gDW
mmol
mmol
mmol
mmol
Tentative units
h^{-1}
mmol/L
mmol gDW/h
mmol gDW/h
mmol gDW/h
mmol/L
mmol gDW (biomass) / mmol (metabolite)
-
mmol (metabolite) / mmol gDW (biomass)

Supplementary Table 2

model	reaction_id
sugar_fermenter	rxn05573
sugar_fermenter	rxn00216
sugar_fermenter	rxn00558
sugar_fermenter	rxn00545
sugar_fermenter	rxn00786
sugar_fermenter	rxn00747
sugar_fermenter	rxn00781
sugar_fermenter	rxn01100
sugar_fermenter	rxn01106
sugar_fermenter	rxn00459
sugar_fermenter	rxn00148
sugar_fermenter	rxn00247
sugar_fermenter	rxn00248
sugar_fermenter	rxn00799
sugar_fermenter	rxn00284
sugar_fermenter	rxn00157
sugar_fermenter	rxn13974
sugar_fermenter	rxn00173
sugar_fermenter	rxn00225
sugar_fermenter	rxn00499
sugar_fermenter	EX_cpd00027_e
sugar_fermenter	EX_cpd00159_e
sugar_fermenter	EX_cpd00047_e
sugar_fermenter	EX_cpd00029_e
sugar_fermenter	EX_cpd00036_e
sugar_fermenter	EX_cpd00067_e
sugar_fermenter	RNF
sugar_fermenter	biomass
sugar_fermenter	piSink
sugar_fermenter	h2oSink
butyrate_producer	rxn05147
butyrate_producer	rxn00216
butyrate_producer	rxn00558
butyrate_producer	rxn00545
butyrate_producer	rxn00786
butyrate_producer	rxn00747
butyrate_producer	rxn00781
butyrate_producer	rxn01100
butyrate_producer	rxn01106
butyrate_producer	rxn00459
butyrate_producer	rxn00148
butyrate_producer	rxn00499
butyrate_producer	rxn05938
butyrate_producer	rxn00173
butyrate_producer	rxn00225
butyrate_producer	rxn00178

butyrate_producer rxn27735
butyrate_producer rxn02167
butyrate_producer rxn00875
butyrate_producer rxn08173
butyrate_producer rxn45849
butyrate_producer EX_cpd00027_e
butyrate_producer EX_cpd00159_e
butyrate_producer EX_cpd00029_e
butyrate_producer EX_cpd00011_e
butyrate_producer EX_cpd11640_e
butyrate_producer EX_cpd00211_e
butyrate_producer EX_cp00067_e
butyrate_producer RNF
butyrate_producer BTCOADH
butyrate_producer biomass
butyrate_producer piSink
butyrate_producer h2oSink
acetogen rxn05147
acetogen rxn00216
acetogen rxn00558
acetogen rxn00545
acetogen rxn00786
acetogen rxn00747
acetogen rxn00781
acetogen rxn01100
acetogen rxn01106
acetogen rxn00459
acetogen rxn00148
acetogen rxn05938
acetogen rxn00173
acetogen rxn00225
acetogen rxn00499
acetogen rxn00690
acetogen rxn01211
acetogen rxn00906
acetogen rxn04954
acetogen rxn06149
acetogen rxn39948
acetogen rxn45849
acetogen rxn08173
acetogen EX_cpd00027_e
acetogen EX_cpd00159_e
acetogen EX_cpd00029_e
acetogen EX_cpd00011_e
acetogen EX_cpd11640_e
acetogen EX_cpd00047_e
acetogen EX_cp00067_e

acetogen	RNF
acetogen	FDH
acetogen	h2T
acetogen	co2T
acetogen	forT
acetogen	biomass
acetogen	piSink
acetogen	h2oSink

reaction_name
D-glucose transport in via proton symport
ATP:D-glucose 6-phosphotransferase
D-glucose-6-phosphate aldose-ketose-isomerase
ATP:D-fructose-6-phosphate 1-phosphotransferase
D-fructose-1,6-bisphosphate D-glyceraldehyde-3-phosphate-lyase (glycerone-phosphate-forming)
D-glyceraldehyde-3-phosphate aldose-ketose-isomerase
D-glyceraldehyde-3-phosphate:NAD+ oxidoreductase (phosphorylating)
ATP:3-phospho-D-glycerate 1-phosphotransferase
2-Phospho-D-glycerate 2,3-phosphomutase
2-phospho-D-glycerate hydro-lyase (phosphoenolpyruvate-forming)
ATP:pyruvate 2-O-phosphotransferase
ATP:oxaloacetate carboxy-lyase (transphosphorylating;phosphoenolpyruvate-forming)
(S)-malate:NAD+ oxidoreductase
(S)-malate hydro-lyase (fumarate-forming)
succinate:NAD+ oxidoreductase
Acetyl-CoA:formate C-acetyltransferase
pyruvate:ferredoxin 2-oxidoreductase (CoA-acetylating)
acetyl-CoA:phosphate acetyltransferase
ATP:acetate phosphotransferase
(S)-Lactate:NAD+ oxidoreductase

RNF
Mock biomass function

D-Glucose-ABC transport
ATP:D-glucose 6-phosphotransferase
D-glucose-6-phosphate aldose-ketose-isomerase
ATP:D-fructose-6-phosphate 1-phosphotransferase
D-fructose-1,6-bisphosphate D-glyceraldehyde-3-phosphate-lyase (glycerone-phosphate-forming)
D-glyceraldehyde-3-phosphate aldose-ketose-isomerase
D-glyceraldehyde-3-phosphate:NAD+ oxidoreductase (phosphorylating)
ATP:3-phospho-D-glycerate 1-phosphotransferase
2-Phospho-D-glycerate 2,3-phosphomutase
2-phospho-D-glycerate hydro-lyase (phosphoenolpyruvate-forming)
ATP:pyruvate 2-O-phosphotransferase
(S)-Lactate:NAD+ oxidoreductase
pyruvate ferredoxin oxidoreductase
acetyl-CoA:phosphate acetyltransferase
ATP:acetate phosphotransferase
Acetyl-CoA:acetyl-CoA C-acetyltransferase

BHBDCLOS-RXN
(S)-3-Hydroxybutanoyl-CoA hydro-lyase
Butanoyl-CoA:acetate CoA-transferase
F(1)-ATPase

RNF
Butanoyl-CoA:acetate CoA-transferase
Mock biomass function

D-Glucose-ABC transport
ATP:D-glucose 6-phosphotransferase
D-glucose-6-phosphate aldose-ketose-isomerase
ATP:D-fructose-6-phosphate 1-phosphotransferase
D-fructose-1,6-bisphosphate D-glyceraldehyde-3-phosphate-lyase (glycerone-phosphate-forming)
D-glyceraldehyde-3-phosphate aldose-ketose-isomerase
D-glyceraldehyde-3-phosphate:NAD+ oxidoreductase (phosphorylating)
ATP:3-phospho-D-glycerate 1-phosphotransferase
2-Phospho-D-glycerate 2,3-phosphomutase
2-phospho-D-glycerate hydro-lyase (phosphoenolpyruvate-forming)
ATP:pyruvate 2-O-phosphotransferase
pyruvate ferredoxin oxidoreductase
acetyl-CoA:phosphate acetyltransferase
ATP:acetate phosphotransferase
(S)-Lactate:NAD+ oxidoreductase
Formate:tetrahydrofolate ligase (ADP-forming)
5,10-Methenyltetrahydrofolate 5-hydrolase (decyclizing)
5,10-methylenetetrahydrofolate:NAD+ oxidoreductase
5-methyltetrahydrofolate:NAD+ oxidoreductase
5-Methyltetrahydrofolate:Corrinoid Co-methyltransferase

F(1)-ATPase

RNF

H2 passive transport
co2 passive transport
formate passive transport
Mock biomass function

equation

D-Glucose + H+ <=> D-Glucose + H+
ATP + D-Glucose <=> ADP + H+ + D-glucose-6-phosphate
D-glucose-6-phosphate <=> D-fructose-6-phosphate
ATP + D-fructose-6-phosphate <=> ADP + H+ + D-fructose-1,6-bisphosphate
D-fructose-1,6-bisphosphate <=> Glycerone-phosphate + Glyceraldehyde3-phosphate
Glyceraldehyde3-phosphate <=> Glycerone-phosphate
NAD + Phosphate + Glyceraldehyde3-phosphate <=> NADH + H+ + 1,3-Bisphospho-D-glycerate
ATP + 3-Phosphoglycerate <=> ADP + 1,3-Bisphospho-D-glycerate
2-Phospho-D-glycerate <=> 3-Phosphoglycerate
2-Phospho-D-glycerate <=> H2O + Phosphoenolpyruvate
ATP + Pyruvate <=> ADP + Phosphoenolpyruvate + H+
ATP + Oxaloacetate <=> ADP + CO2 + Phosphoenolpyruvate
NAD + L-Malate <=> NADH + Oxaloacetate + H+
L-Malate <=> H2O + Fumarate
NAD + Succinate <-- NADH + H+ + Fumarate
Acetyl-CoA + Formate <-- CoA + Pyruvate
CO2 + Acetyl-CoA + H+ + 2.0 Reducedferredoxin <=> CoA + Pyruvate + 2.0 Oxidizedferredoxin
Phosphate + Acetyl-CoA <=> CoA + Acetylphosphate
ATP + Acetate <-- ADP + Acetylphosphate
NAD + L-Lactate <-- NADH + Pyruvate + H+
D-Glucose <=>
L-Lactate <=>
Formate <=>
Acetate <=>
Succinate -->
H+ <=>
NAD + 3.0 H+ + 2.0 Reducedferredoxin <=> NADH + 2.0 H+ + 2.0 Oxidizedferredoxin
3.0 ATP + 2.0 NADH + 2.0 Acetyl-CoA + 2.0 H+ --> 2.0 NAD + 3.0 ADP + 2.0 CoA
Phosphate <=>
H2O <=>
H2O + ATP + D-Glucose --> ADP + Phosphate + D-Glucose + H+
ATP + D-Glucose <=> ADP + H+ + D-glucose-6-phosphate
D-glucose-6-phosphate <=> D-fructose-6-phosphate
ATP + D-fructose-6-phosphate <=> ADP + H+ + D-fructose-1,6-bisphosphate
D-fructose-1,6-bisphosphate <=> Glycerone-phosphate + Glyceraldehyde3-phosphate
Glyceraldehyde3-phosphate <=> Glycerone-phosphate
NAD + Phosphate + Glyceraldehyde3-phosphate <=> NADH + H+ + 1,3-Bisphospho-D-glycerate
ATP + 3-Phosphoglycerate <=> ADP + 1,3-Bisphospho-D-glycerate
2-Phospho-D-glycerate <=> 3-Phosphoglycerate
2-Phospho-D-glycerate <=> H2O + Phosphoenolpyruvate
ATP + Pyruvate <=> ADP + Phosphoenolpyruvate + H+
NAD + L-Lactate <=> NADH + Pyruvate + H+
CO2 + Acetyl-CoA + H+ + Reducedferredoxin <-- CoA + Pyruvate + Oxidizedferredoxin
Phosphate + Acetyl-CoA <=> CoA + Acetylphosphate
ATP + Acetate <-- ADP + Acetylphosphate
2.0 Acetyl-CoA <=> CoA + Acetoacetyl-CoA

NADH + H+ + Acetoacetyl-CoA <=> NAD + (S)-3-Hydroxybutyryl-CoA
(S)-3-Hydroxybutyryl-CoA --> H2O + Crotonyl-CoA
Acetate + Butyryl-CoA --> Acetyl-CoA + Butyrate
ADP + Phosphate + 4.0 H+ <=> H2O + ATP + 3.0 H+
2.0 Oxidizedferredoxin + H2 <=> 2.0 H+ + 2.0 Reducedferredoxin
D-Glucose <=>
L-Lactate <=>
Acetate <=>
CO2 <=>
H2 <=>
Butyrate -->
H+ <=>
NAD + 3.0 H+ + 2.0 Reducedferredoxin <=> NADH + 2.0 H+ + 2.0 Oxidizedferredoxin
2.0 NADH + 2.0 H+ + Crotonyl-CoA + Oxidizedferredoxin --> 2.0 NAD + Butyryl-CoA + Reducedferredoxin
3.0 ATP + 2.0 NADH + 2.0 Acetyl-CoA + 2.0 H+ --> 2.0 NAD + 3.0 ADP + 2.0 CoA
Phosphate <=>
H2O <=>
H2O + ATP + D-Glucose --> ADP + Phosphate + D-Glucose + H+
ATP + D-Glucose <=> ADP + H+ + D-glucose-6-phosphate
D-glucose-6-phosphate <=> D-fructose-6-phosphate
ATP + D-fructose-6-phosphate <=> ADP + H+ + D-fructose-1,6-bisphosphate
D-fructose-1,6-bisphosphate <=> Glycerone-phosphate + Glyceraldehyde3-phosphate
Glyceraldehyde3-phosphate <=> Glycerone-phosphate
NAD + Phosphate + Glyceraldehyde3-phosphate <=> NADH + H+ + 1,3-Bisphospho-D-glycerate
ATP + 3-Phosphoglycerate <=> ADP + 1,3-Bisphospho-D-glycerate
2-Phospho-D-glycerate <=> 3-Phosphoglycerate
2-Phospho-D-glycerate <=> H2O + Phosphoenolpyruvate
ATP + Pyruvate <=> ADP + Phosphoenolpyruvate + H+
CO2 + Acetyl-CoA + H+ + Reducedferredoxin <-- CoA + Pyruvate + Oxidizedferredoxin
Phosphate + Acetyl-CoA <=> CoA + Acetylphosphate
ATP + Acetate <-- ADP + Acetylphosphate
NAD + L-Lactate <-- NADH + Pyruvate + H+
ATP + Formate + Tetrahydrofolate <=> ADP + Phosphate + 10-Formyltetrahydrofolate
H2O + 5-10-Methenyltetrahydrofolate <=> H+ + 10-Formyltetrahydrofolate
NAD + 5-10-Methylenetetrahydrofolate <=> NADH + 5-10-Methenyltetrahydrofolate
NAD + 5-Methyltetrahydrofolate <=> NADH + H+ + 5-10-Methylenetetrahydrofolate
H+ + 5-Methyltetrahydrofolate + Corrinoid --> Tetrahydrofolate + Methylcorrinoid
CoA + CO2 + H+ + Reducedferredoxin + Methylcorrinoid --> H2O + Acetyl-CoA + Oxidizedferredoxin + Corrinoid
2.0 Oxidizedferredoxin + H2 --> 2.0 H+ + 2.0 Reducedferredoxin
ADP + Phosphate + 4.0 H+ <=> H2O + ATP + 3.0 H+
D-Glucose <=>
L-Lactate <=>
Acetate <=>
CO2 <=>
H2 <=>
Formate <=>
H+ <=>

NAD + 3.0 H+ + 2.0 Reducedferredoxin <=> NADH + 2.0 H+ + 2.0 Oxidizedferredoxin
NAD + 2.0 Formate + 2.0 Oxidizedferredoxin <=> NADH + 2.0 CO2 + H+ + 2.0 Reducedferredoxin
H2 <=> H2
CO2 <=> CO2
Formate <=> Formate
3.0 ATP + 2.0 NADH + 2.0 Acetyl-CoA + 2.0 H+ --> 2.0 NAD + 3.0 ADP + 2.0 CoA
Phosphate <=>
H2O <=>

Supplementary Table 3

ID	Reactants
glycolysis_cf	glucose_out:1
pyruvateS_cf	pep_cf:1, proton_cf:1
formateP_cf	pyruvate_cf:1
succinateP_cf	pep_cf:1, nadh_cf:2, proton_cf:2
lactateP_cf	pyruvate_cf:1, proton_cf:1, nadh_cf:1
acetateP_cf	pyruvate_cf:1
rnf_cf	proton_cf:3, ferredoxinrd_cf:2
biomass_cf	accoa_cf:2, atp_cf:3, nadh_cf:2, proton_cf:2
glycolysis_bp	glucose_out:1
lactateP_bp	pyruvate_bp:1, proton_bp:1, nadh_bp:1
co2P_bp	pyruvate_bp:1
acetateP_bp	accoa_bp:1
butyrateP_bp	accoa_bp:1, acetate_out:1, nadh_bp:3, proton_bp:3
rnf_bp	proton_bp:3, ferredoxinrd_bp:2
atpase_bp	proton_out:4
hydrogenase_bp	proton_bp:2, ferredoxinrd_bp:2
biomass_bp	accoa_bp:2, atp_bp:4, nadh_bp:2, proton_bp:2
formateD_ac	co2_out:2, ferredoxinrd_ac:2, proton_ac:2, nadh_ac:1
WL_ac	formate_ac:1, atp_ac:1, proton_ac:4, nadh_ac:2, co2_out:1, ferredoxinrd_ac:1
glycolysis_ac	glucose_out:1
lactateP_ac	pyruvate_ac:1, proton_ac:1, nadh_ac:1
co2P_ac	pyruvate_ac:1
acetateP_ac	accoa_ac:1
rnf_ac	proton_ac:3, ferredoxinrd_ac:2
atpase_ac	proton_out:4
hydrogenase_ac	proton_ac:2, ferredoxinrd_ac:2
forT	formate_ac:1
biomass_ac	accoa_ac:2, atp_ac:4, nadh_ac:2, proton_ac:2

Products	Forward_Rate	Reversed_Rate
pep_cf:2, nadh_cf:2, proton_cf:4	1	0
pyruvate_cf:1, atp_cf:1	1	0
formate_out:1, accoa_cf:1	0.5	0
succinate_out:1, atp_cf: 1	0.001	0
lactate_out:1	0.01	0
acetate_out:1, ferredoxinrd_cf:2, proton_cf:1, atp_cf:1	0.055	0
nadh_cf:1, proton_out:3	0.1	0
biomass_cf:1	1	0
pyruvate_bp:2, nadh_bp:2, proton_bp:2, atp_bp:2	1	0
lactate_out:1	0.2	0.1
accoa_bp:1, ferredoxinrd_bp:1, proton_bp:1, co2_out:1	0.5	0
atp_bp:1, acetate_out:1	0.6	0.1
butyrate_out:1, ferredoxinrd_bp:1	0.7	0
nadh_bp:1, proton_out:3	0.2	0
atp_bp:1, proton_bp:3	0.5	0.1
h2_out:1	1	0.1
biomass_bp:1	1	0
formate_ac:2	0.7	0
accoa_ac:1	1	0
pyruvate_ac:2, nadh_ac:2, proton_ac:2, atp_ac:2	0.1	0
lactate_out:1	0.01	0
accoa_ac:1, ferredoxinrd_ac:1, proton_ac:1, co2_out:1	1	0
atp_ac:1, acetate_out:1	0.6	0.1
nadh_ac:1, proton_out:3	1	0
atp_ac:1, proton_ac:3	0.5	0.1
h2_out:1	0.1	1
formate_out:1	0.1	0.1
biomass_ac:1	1	0